Atomistic Approach toward Selective Photocatalytic Oxidation of a Mustard-Gas Simulant: A Case Study with Heavy-Chalcogen-Containing PCN-57 Analogues

Subhadip Goswami,[†] Claire E. Miller,[†] Jenna L. Logsdon,[†] Cassandra T. Buru,[†] Yi-Lin Wu,[†,∥] David N. Bowman,[‡] Timur Islamoglu,[†] Abdullah M. Asiri,[§] Christopher J. Cramer,[‡] Michael R. Wasielewski,[†,∥] Joseph T. Hupp,[†,∥] and Omar K. Farha*[,†,§]

[†]Department of Chemistry and [∥]Argonne-Northwestern Solar Energy Research (ANSER) Center, Northwestern University, 2145 Sheridan Road, Evanston, Illinois 60208, United States

[‡]Department of Chemistry, Chemical Theory Center, and Supercomputing Institute, University of Minnesota, Minneapolis, Minnesota 55455-0431, United States

[§]Department of Chemistry, King Abdulaziz University, Jeddah 21589, Saudi Arabia

* Supporting Information

ABSTRACT: Here we describe the synthesis of two Zr-based benzothiadiazole- and benzoselenadiazole-containing metal−organic frameworks (MOFs) for the selective photocatalytic oxidation of the mustard gas simulant, 2-chloroethyl ethyl sulfide (CEES). The photophysical properties of the linkers and MOFs are characterized by steady-state absorption and emission, time-resolved emission, and ultrafast transient absorption spectroscopy. The benzoselenadiazole-containing MOF shows superior catalytic activity compared to that containing benzothiadiazole with a half-life of 3.5 min for CEES oxidation to nontoxic 2-chloroethyl ethyl sulfoxide (CEESO). Transient absorption spectroscopy performed on the benzoselenadiazole linker reveals the presence of a triplet excited state, which decays with a lifetime of 9.4 μs, resulting in the generation of singlet oxygen for photocatalysis. This study demonstrates the effect of heavy chalcogen substitution within a porous framework for the modulation of photocatalytic activity.

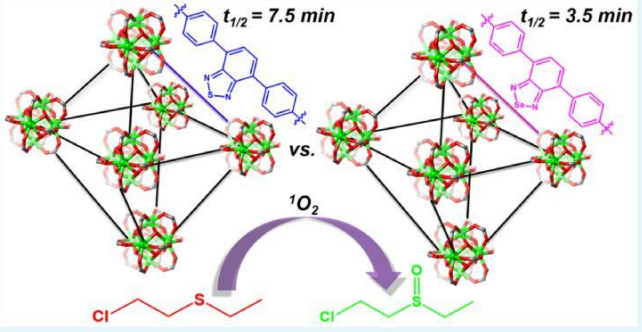

KEYWORDS: metal−organic framework, photocatalysis, chemical warfare agents, sulfur mustard, transient absorption

First used in World War I, chemical warfare agents (CWAs) a subclass of weapons of mass destruction (WMDs) have been a persistent threat to mankind.[1] Sulfur mustard or mustard gas (HD) [bis(2-chloroethyl) sulfide] is one example of a CWA that can be lethal, because of its vesicant properties. In addition to causing severe blistering on exposed skin, sulfur mustard can irritate lungs and eyes.[2] Despite the nearly universal imposition of restrictions on the use of CWAs, under the 1993 Chemical Weapons Convention (C.W.C.),[3] recent news articles suggest that production and stockpiling of sulfur mustard, as well as use as a chemical weapon, are still occurring.[4] Therefore, it is of paramount interest to discover efficient materials to detoxify this blistering agent. In general, there are three major routes for the detoxification of sulfur mustard, namely (1) dehydrohalogenation, (2) hydrolysis, and (3) oxidation; however, each of these processes comes with its own limitations.[2,5,6] We believe partial oxidation of HD to its sulfoxide analogue, HD-O, is the most promising deactivation pathway. However, control of HD oxidation is crucial because overoxidation can lead to a sulfone derivative, which itself is a blistering agent, and depending on the means of exposure, is ca. 0.1 to 0.5 times as toxic HD.[7] In contrast, the half-oxidized degradation product (i.e., the sulfoxide) is considered to be only slightly toxic.[7] Singlet oxygen ($^1O_2$) is a popular green oxidizing agent that has shown promising results for the detoxification of sulfur mustard. Because of the extensive research on singlet oxygen photo-sensitizers, a variety of chromophores are available to sensitize the production of singlet oxygen; porphyrins, chlorin, and phthalocyanines are some examples.[8] Efficient photocatalysis is achievable by both homogeneous and heterogeneous systems, with the latter offering the following comparative advantages:

(1) ease of separation after catalysis by simple filtration, (2) recyclability, (3) the opportunity to scan over several solvents to optimize the reaction of interest,[9] and (4) easier incorporation into filters and other devices/technologies.

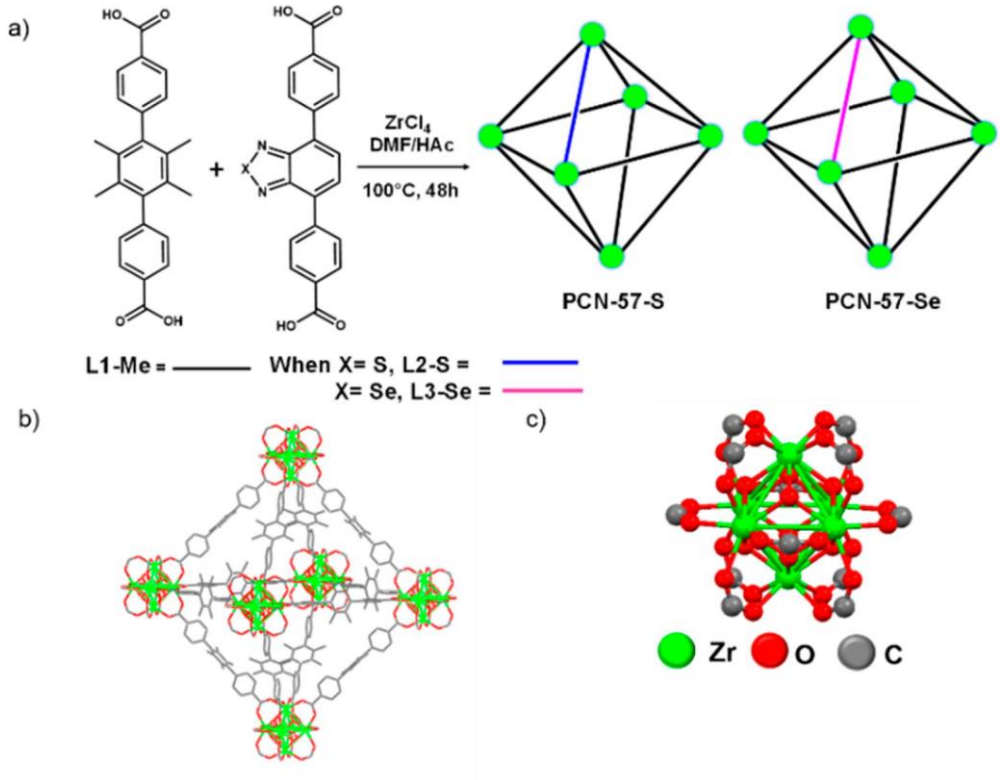

Figure 1. (a) Schematic representation of the synthesis of PCN-57-S and PCN-57-Se using a mixed ligand approach. (b) Structure of PCN-57.[10] (c) Structure of the Zr_6 node of PCN-57.

Recently, metal−organic frameworks (MOFs) have been used as heterogeneous scaffolds for catalytically active chromophores in order to improve the catalyst performance by site isolation. MOFs are crystalline and porous 3D networks formed by coordination of metal nodes and multitopic organic bridging linkers.[11−16] The tunability of the organic linkers and metal ions makes these materials highly sought after for applications including gas storage/separation,[17] catalysis,[13,18,19] drug delivery,[20] photodynamic therapy,[21] energy transfer,[22−24] and chemical sensing.[25] The stability of MOFs is an important property especially for use and reuse of MOFs as a catalyst. Zirconium(IV) containing MOFs (Zr-MOFs) exhibit high stability compared to MOFs made from other metals due to the high charge density on the metal ion which in turn makes the coordination bonds between Zr(IV) and carboxylates very strong.[26] We have previously reported the use of a porphyrin photosensitizer in a Zr_6-based MOF PCN-222/MOF-545, to photocatalyze the oxidation of mustard gas simulant 2-chloroethyl ethyl sulfide (CEES) to 2-chloroethyl ethyl sulfoxide (CEESO) with a blue LED at a half-life ($t_{1/2}$) of 13 min.[6] The pyrene containing mesoporous MOF, NU-1000, showed catalytic activity for the partial oxidation of CEES itself under UV light ($t_{1/2}$ = 6 min).[5] The catalytic performance of NU-1000 was further improved ($t_{1/2}$ = 3.5 min) when fullerene-based photosensitizers were postsynthetically incorporated in the MOF.[27] Although significant strides have been made toward developing MOF-based photocatalysts for the detox-ification of sulfur mustard, there is a need to design new catalytic materials to achieve close-to-instantaneous detoxifica-tion as well as to extract design rules.

Herein, we report: (a) the synthesis, using a mixed-ligand approach, of versions of PCN-57 that are partially substituted with benzoselenadiazole (PCN-57-Se) or benzothiadiazole (PCN-57-S) linkers (Figure 1), and (b) evaluation of the efficacy of these new materials for the selective photocatalytic partial oxidation of 2-chloroethyl ethyl sulfide (CEES) to 2-chloroethyl ethyl sulfoxide (CEESO). Notably, PCN-57-Se is a more effective photocatalyst ($t_{1/2}$ = 3.5 min) than PCN-57-S ($t_{1/2}$ = 7.5 min). While the half-lives for the photocatalytic oxidation of CEES with PCN-57-Se are similar to that of the fullerene containing NU-1000,[27] lower catalyst loading (0.1 mol % based on chromophore) is required when compared to fullerene containing NU-1000 (0.7 mol %). Additionally, to the best of our knowledge this is the first report of photocatalytic detoxification of a sulfur-mustard simulant using a UiO-type framework where catalytic rates can be controlled by mere substitution of heteroatoms in the framework.

Benzothiadiazole- and benzoselenadiazole-based linkers were selected because of the known ability of the isolated diazoles to sensitize the photochemical formation of singlet oxygen.[28,29] PCN-57-S and PCN-57-Se were synthesized using a mixed linker approach by direct synthesis of the MOF with 2′,3′,5′,6′-tetramethylterphenyl-4,4″-dicarboxylate (L1-Me, $[TPDC\text{-}4CH_3]^{2-}$), as well as, either L2-S and L3-Se (details in Supporting Information). Briefly, PCN-57 was synthesized by heating a mixture of $ZrOCl_2{\cdot}8H_2O$ and $TPDC\text{-}4CH_3$ in the presence of benzoic acid as modulator at 100 °C for 24 h in N,N-dimethylformamide (DMF).[10] Both PCN-57-S and PCN-57-Se were synthesized by taking the respective linkers (L2-S or L3-Se) and $TPDC\text{-}4CH_3$ in 1:4 ratio in DMF, $ZrCl_4$ as metal source, acetic acid as modulator and heating the mixtures at 100 °C for 48 h. To confirm the ratio of linkers in the final structures by ^1H NMR, the MOF samples were digested in a D_2SO_4/DMSO-d_6 solution. The ratio between the protons of

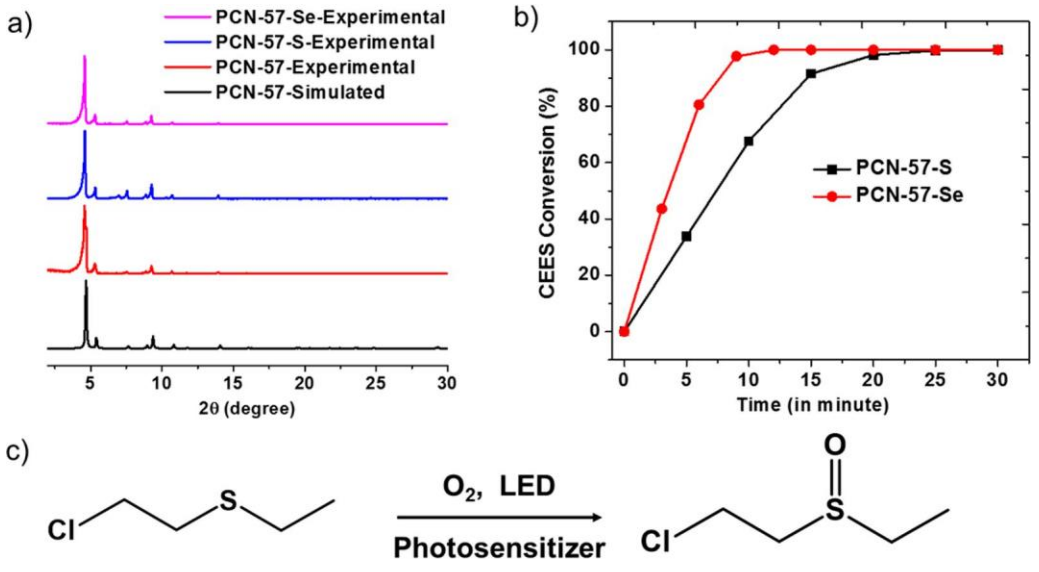

Figure 2. (a) Comparison of PXRD patterns of simulated PCN-57 with as-synthesized PCN-57, PCN-57-S, and PCN-57-Se. (b) Photooxidation profile of CEES with PCN-57-S(UV LED) and PCN-57-Se (violet LED). (c) Reaction scheme for the photooxidation of CEES in the presence of oxygen.

the linker TPDC-4CH_3 and L2-S or L3-Se shows that the linker incorporation is indeed in agreement with the ratio of the linkers used in the syntheses (Figures S9 and S10). Inductively coupled plasma optical emission spectroscopy (ICP-OES) of PCN-57-S and PCN-57-Se showed incorporation of one S and one Se per Zr_6 node respectively which confirms the expected value (~1.2) considering 20% incorporation of the linker with the formula $Zr_6O_4(OH)_4$(TPDC-4CH_3)$_{4.8}$(L-X)$_{1.2}$ where X = S or Se. Scanning electron microscopy with energy dispersive X-ray spectroscopy (SEM-EDX) showed uniform distribution of Zr and S/Se throughout the MOF crystals (Figure S20−S22). The crystallinity of each sample was verified by powder X-ray diffraction (PXRD) and similar PXRD patterns were observed for all MOFs, suggesting that they are isostructural with PCN-57 (Figure 2a). The permanent porosity of the samples were examined by N_2 isotherm measurements at 77 K after activation at 120 °C under vacuum for 12 h. As expected, all the materials showed typical type I reversible isotherms. PCN-57 has the highest Brunauer−Emmett−Teller (BET) surface area (3300 m^2/g) among the three, with PCN-57-S and PCN-57-Se having surface areas of 2400 and 2800 m^2/g, respectively (Figure S11).

The ground-state absorption spectra of the MOFs were examined via diffuse reflectance UV−vis measurements (Figure S13a). PCN-57 showed absorption between 200 and 300 nm with maximum absorption (λ_{max}) at 283 nm. As expected, the incorporation of chromophores L2-S and L3-Se red-shifted the MOF absorption spectra into the visible region, with the shift being greater for PCN-57-Se (absorption onset at ~500 nm) than for PCN-57-S. This is in line with red-shifted absorption of Se-containing π-conjugated systems compared to S-containing systems (Figure S15a).[30] The maximum emission wavelength (λ_{max}) for the MOFs also follows the order of PCN-57-Se (512 nm) > PCN-57-S (486 nm) > PCN-57 (351 nm) (Figure S13b).

On the basis of the absorption spectra of MOFs, a UV LED (λ_{max} = 395 nm) and a purple LED (λ_{max} = 405 nm) were chosen for PCN-57-S and PCN-57-Se respectively to perform photocatalytic oxidation of CEES. Note here, the combined power density of the LEDs was maintained at 865 mW/cm^2 in both cases. The progress of the reaction was monitored by GC-FID and the product obtained was analyzed with NMR (^{1}H and ^{13}C) spectroscopy. Under optimized condition when 0.1 mol % PCN-57-Se (based on the 20% L3-Se loading) was used, the reaction was found to go to completion within 12 min with a half-life of 3.5 min (Figure 2b). In contrast, under the same conditions, PCN-57-S requires 25 min to achieve 100% conversion of the starting material to CEESO. The NMR spectra confirm selective oxidation of CEES to CEESO (Figures S14 and S15). The unsubstituted PCN-57 showed no activity since it lacks absorbance at the excitation wavelength. Therefore, we can conclude that L2-S and L3-Se linkers are responsible for the enhanced photocatalytic activity of PCN-57-S and PCN-57-Se, not the TPDC-4CH_3 linker. The photocatalytic reaction using only the linkers, L2-S and L3-Se, in solution showed the same trend as their respective MOFs, L3-Se shows faster catalytic oxidation compared to L2-S (Figure S16).

Given that PCN-57-Se was proven to be a superior catalyst among the three MOFs studied, detailed characterizations related to the heterogeneous photocatalysis were performed using this sample. In an effort to understand the effect of light and oxygen, control experiments were performed. In both cases (i.e., only light or only oxygen), less than 10% conversion of the starting material was observed over 30 min, suggesting that both light and oxygen are essential to perform the catalysis (Figure S19). The heterogeneous nature of the catalyst was confirmed by filtering the catalyst from the reaction mixture after the completion of the reaction and performing the ICP-OES measurement with the filtrate. The absence of Zr and Se proved that there was no leaching of the catalyst from the framework during the reaction and the catalysis is heteroge-neous in nature. Additionally, both ^{1}H and ^{13}C NMR measurements of the filtrate showed absence of TPDC-4CH_3 or L3-Se, providing additional evidence that PCN-57-Se stayed intact during the reaction. PCN-57-Se catalyst was also tested for recyclability. The same sample showed the conversion of CEES to CEESO with excellent yield (>99% yield) for four consecutive cycles (Figure S18). PXRD of the filtered catalysts

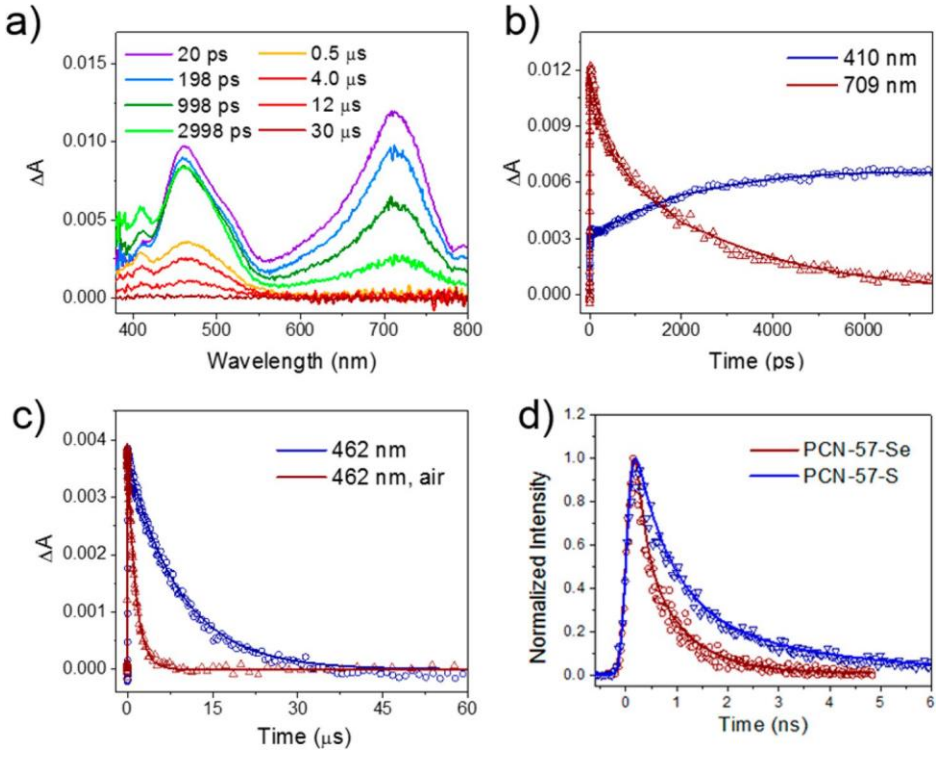

Figure 3. (a) Combined fsTA and nsTA spectra of L3-Se-CO_2Et in deaerated CH_2Cl_2 recorded at time delays indicated in the legends after laser excitation. (b) Kinetic fits at selected wavelengths from fsTA in panel a showing the process of intersystem crossing in τ = 2.8 ± 0.3 ns. (c) Single-wavelength kinetics from nsTA in panel a showing the decay of triplet excited state in the absence (τ = 9.39 ± 0.08 µs) or presence (τ = 1.41 ± 0.01 µs) of air. (d) Time-resolved fluorescence kinetics at 500 nm for PCN-57-S (τ = 1.1 ± 0.2 ns) and PCN-57-Se (τ = 0.6 ± 0.1 ns).

(tested for both PCN-57-S and PCN-57-Se) demonstrated that the structure and the crystallinity of the material remain unaltered after the catalysis (Figure S17). Considering these data, we affirm that the framework is stable under the photocatalytic conditions.

We relied upon femto- and nanosecond transient absorption (fsTA and nsTA) spectroscopy to gain a deeper understanding of excited-state dynamics of L3-Se-CO_2Et and L2-S-CO_2Et in dichloromethane and to therefore understand the photo-catalytic activity of the MOFs in detail. The ester protected linkers were selected over the dicarboxylic acid containing linkers due to their better solubility in organic solvents. For L3-Se-CO_2Et, photoexcitation with 302 nm, 150 fs laser pulses resulted in strong singlet excited state absorption at 460 and 710 nm which decayed with a time constant of 2.8 ± 0.3 ns, concomitant with the growth of new features at 410 and 460 nm (Figure 3a, b). The excited state associated with this new feature decays in 9.39 ± 0.08 µs in the deaerated solution by nsTA. In the presence of air, the excited state lifetime decreased to 1.41 ± 0.01 µs (Figure 3c). The long lifetime and sensitivity to molecular oxygen suggest the triplet nature of this excited state is formed via intersystem crossing, possibly facilitated by the spin−orbit coupling effect (i.e., "heavy-atom effect") of selenium.[31] The assignment is further supported by the resemblance of the transient spectra to triplet-state absorption predicted by linear-response time-dependent density functional theory (LR-TD-DFT; Figure S26). For L2-S-CO_2Et, similar excited-state absorption was observed at 430 and 690 nm upon excitation that is blue-shifted compared to L3-Se-CO_2Et and decayed with a time constant of 6.0 ± 0.1 ns (Figure S23). However, no detectable signature of triplet excited-state absorption was observed for L2-S-CO_2Et within the experimental time scale. In both the cases the observed excited state absorptions for the linkers match the predicted spectra from DFT calculations (Section S16).

The energy difference between the prominent low energy excitation peaks for the excited singlet and triplet species, in going from ground to relaxed geometry, indicates that the singlet and triplet excited state absorptions are significantly impacted by vibrational relaxation (Figure S26). The most prominent difference in geometry between the ground singlet and both the excited singlet and triplet states is a flattening of dihedral angles between the central benzoselenadiazole/benzothiadiazole ring and the flanking phenyl groups. According to DFT calculations, the dihedral angles between rings range from 36.9 to 38.7° (benzothiadiazole) and 38.8 to 40.7° (benzoselenadiazole) in the singlet ground state. In the lowest-energy excited singlet state, the range is reduced to 21.2−21.7° (benzothiadiazole) and 24.7−25.6° (benzoselenadiazole), and in the triplet state, these ranges become 18.7−19.0° (benzothiadiazole) and 24.1−24.9° (benzoselenadiazole).

The excited-state dynamics of the MOFs were probed with time-resolved fluorescence spectroscopy; since the strong light scattering of the solid samples, unfortunately, obstructed the collection of transient absorption signals. The fluorescence lifetimes for the PCN-57-Se and PCN-57-S samples were found to be 0.6 ± 0.1 ns and 1.1 ± 0.2 ns, respectively. The shorter lifetime, compared to the ester ligands, can be ascribed to the decreased S_0−S_1 energy gap in the MOF samples, manifested by the red shift in steady-state emission spectra (Figure S25b). Additionally, coordination of the linkers to the metal center could also contribute to shortening of the excited state lifetime in the MOF.[32,33] Most importantly, the faster singlet decay in PCN-57-Se is in line with rapid intersystem crossing to form

the triplet excited state as observed for the ester protected ligand. The population of the triplet excited state yields efficient singlet oxygen production and subsequent photocatalysis.

In conclusion, we have found that the sulfur mustard simulant, CEES, can be selectively photocatalytically oxidized to nontoxic monooxygenated product CEESO using singlet oxygen ($^1O_2$) generated by highly porous, crystalline benzoselenadiazole and benzothiadiazole substituted PCN-57 frameworks (PCN-57-Se and PCN-57-S, respectively). Under violet LED irradiation and 1 atm O_2, PCN-57-Se catalyzes the photooxidation with 100% conversion within 12 min ($t_{1/2}$= 3.5 min), and PCN-57-S completes the reaction in 25 min ($t_{1/2}$= 7.5 min) under UV irradiation. The retention of crystallinity of the MOF samples and the absence of leaching of the catalyst during reaction evince the heterogeneous nature of the catalyst. A detailed study of steady-state and time-resolved emission spectroscopy, carried out with ester-protected linkers and with MOF samples, and supported by computations, points to efficient excited-state singlet-to-triplet intersystem crossing for the selenium containing samples as a key factor for the higher catalytic activity of PCN-57-Se. An additional factor may be better energy matching of the triplet photoexcited-state of PCN-57-Se to the O_2 triplet-to-singlet transition at E = 1.63 eV (λ = 762 nm). We believe this class of materials is promising for the heterogeneous photocatalytic detoxification of CWAs and has future potential in catalyzing other important reactions because of the rich photoredox properties of the chromophores.

ASSOCIATED CONTENT

* Supporting Information

Specifics on materials used, synthesis of the linkers and MOFs, details of characterization, instrumentation, and "computational methods and results" (PDF)

AUTHOR INFORMATION

Corresponding Author

*E-mail: o-farha@northwestern.edu.

ORCID

Subhadip Goswami: 0000-0002-8462-9054

Cassandra T. Buru: 0000-0001-6142-8252

David N. Bowman: 0000-0002-0826-8525

Timur Islamoglu: 0000-0003-3688-9158

Christopher J. Cramer: 0000-0001-5048-1859

Michael R. Wasielewski: 0000-0003-2920-5440

Joseph T. Hupp: 0000-0003-3982-9812

Omar K. Farha: 0000-0002-9904-9845

Notes

The authors declare no competing financial interest.

ACKNOWLEDGMENTS

O.K.F. and J.T.H. (Project W911NF-13-1-0229) gratefully acknowledge support by the Army Research Office. This work was supported by the Chemical Sciences, Geosciences, and Biosciences Division, Office of Basic Energy Sciences, U.S. Department of Energy (DOE), under Grants DE-FG02-99ER14999 (M.R.W.) and SciDAC DE-SC0008666 (C.J.C. and D.N.B.). S.G. thank Yuexing Cui for help with the diffuse-reflectance UV measurements and Dr. Hyeju Choi for help with the SEM measurements. The SEM images in this work obtained by using the EPIC facility (NUANCE Center, Northwestern University), which has received support from the MRSEC program (NSF DMR-1121262) at the Materials Research Center; the International Institute for Nanotechnol-ogy (IIN); and the State of Illinois, through the IIN. We also acknowledge the Minnesota Supercomputing Institute (MSI) at the University of Minnesota for providing computational resources.

REFERENCES

(1) Ghabili, K.; Agutter, P. S.; Ghanei, M.; Ansarin, K.; Panahi, Y.; Shoja, M. M. Sulfur Mustard Toxicity: History, Chemistry, Pharmacokinetics, and Pharmacodynamics. Crit. Rev. Toxicol. 2011, 41, 384−403.

(2) Smith, B. M. Catalytic Methods for the Destruction of Chemical Warfare Agents under Ambient Conditions. Chem. Soc. Rev. 2008, 37, 470−478.

(3) Organisation for the Prohibition of Chemical Weapons. Chemical Weapons Convention. Https://Www.Opcw.Org/Chemical-Weaponsconvention/ (Accessed Aug 19, 2016).

(4) (A) Hess, G. UN Says Syria and Islamic State Used Chemical Weapons. Chemical and Engineering News, August 2016. (B) Fassihi, F. U.N. Report Finds Chemical Weapons Used by Syrian Regime, Islamic State. The Wall Street Journal, August 2016.

(5) Liu, Y.; Buru, C. T.; Howarth, A. J.; Mahle, J. J.; Buchanan, J. H.; DeCoste, J. B.; Hupp, J. T.; Farha, O. K. Efficient and Selective Oxidation of Sulfur Mustard Using Singlet Oxygen Generated by a Pyrene-Based Metal-Organic Framework. J. Mater. Chem. A 2016, 4, 13809−13813.

(6) Liu, Y.; Howarth, A. J.; Hupp, J. T.; Farha, O. K. Selective Photooxidation of a Mustard-Gas Simulant Catalyzed by a Porphyrinic Metal−Organic Framework. Angew. Chem., Int. Ed. 2015, 54, 9001− 9005.

(7) Munro, N. B.; Talmage, S. S.; Griffin, G. D.; Waters, L. C.; Watson, A. P.; King, J. F.; Hauschild, V. The Sources, Fate, and Toxicity of Chemical Warfare Agent Degradation Products. Environ. Health Perspect. 1999, 107, 933.

(8) Kimel, S.; Tromberg, B. J.; Roberts, W. G.; Berns, M. W. Singlet Oxygen Generation of Porphyrins, Chlorins, and Phthalocyanines. Photochem. Photobiol. 1989, 50, 175−183.

(9) Fox, M. A.; Dulay, M. T. Heterogeneous Photocatalysis. Chem. Rev. 1993, 93, 341−357.

(10) Jiang, H.-L.; Feng, D.; Liu, T.-F.; Li, J.-R.; Zhou, H.-C. Pore Surface Engineering with Controlled Loadings of Functional Groups Via Click Chemistry in Highly Stable Metal−Organic Frameworks. J. Am. Chem. Soc. 2012, 134, 14690−14693.

(11) Furukawa, H.; Cordova, K. E.; O'Keeffe, M.; Yaghi, O. M. The Chemistry and Applications of Metal-Organic Frameworks. Science 2013, 341, 1230444.

(12) Guillerm, V.; Kim, D.; Eubank, J. F.; Luebke, R.; Liu, X.; Adil, K.; Lah, M. S.; Eddaoudi, M. A Supermolecular Building Approach for the Design and Construction of Metal-Organic Frameworks. Chem. Soc. Rev. 2014, 43, 6141−6172.

(13) Lee, J.; Farha, O. K.; Roberts, J.; Scheidt, K. A.; Nguyen, S. T.; Hupp, J. T. Metal-Organic Framework Materials as Catalysts. Chem. Soc. Rev. 2009, 38, 1450−1459.

(14) Chen, B.; Eddaoudi, M.; Hyde, S. T.; O'Keeffe, M.; Yaghi, O. M. Interwoven Metal-Organic Framework on a Periodic Minimal Surface with Extra-Large Pores. Science 2001, 291, 1021−1023.

(15) Kitagawa, S.; Kitaura, R.; Noro, S.-i. Functional Porous Coordination Polymers. Angew. Chem., Int. Ed. 2004, 43, 2334−2375.

(16) Islamoglu, T.; Goswami, S.; Li, Z.; Howarth, A. J.; Farha, O. K.; Hupp, J. T. Postsynthetic Tuning of Metal−Organic Frameworks for Targeted Applications. Acc. Chem. Res. 2017, 50, 805−813.

(17) Li, J.-R.; Kuppler, R. J.; Zhou, H.-C. Selective Gas Adsorption and Separation in Metal-Organic Frameworks. Chem. Soc. Rev. 2009, 38, 1477−1504.

(18) Liu, J.; Chen, L.; Cui, H.; Zhang, J.; Zhang, L.; Su, C.-Y. Applications of Metal-Organic Frameworks in Heterogeneous Supramolecular Catalysis. Chem. Soc. Rev. 2014, 43, 6011−6061.
(19) Rimoldi, M.; Howarth, A. J.; DeStefano, M. R.; Lin, L.; Goswami, S.; Li, P.; Hupp, J. T.; Farha, O. K. Catalytic Zirconium/ Hafnium-Based Metal−Organic Frameworks. ACS Catal. 2017, 7, 997−1014.
(20) Qin, J.-S.; Du, D.-Y.; Li, W.-L.; Zhang, J.-P.; Li, S.-L.; Su, Z.-M.; Wang, X.-L.; Xu, Q.; Shao, K.-Z.; Lan, Y.-Q. N-Rich Zeolite-Like Metal-Organic Framework with Sodalite Topology: High Co2 Uptake, Selective Gas Adsorption and Efficient Drug Delivery. Chem.Sci. 2012, 3, 2114−2118.
(21) Lu, K.; He, C.; Lin, W. Nanoscale Metal−Organic Framework for Highly Effective Photodynamic Therapy of Resistant Head and Neck Cancer. J. Am. Chem. Soc. 2014, 136, 16712−16715.
(22) Dolgopolova, E. A.; Rice, A. M.; Smith, M. D.; Shustova, N. B. Photophysics, Dynamics, and Energy Transfer in Rigid Mimics of Gfp-Based Systems. Inorg. Chem. 2016, 55, 7257−7264.
(23) Lee, C. Y.; Farha, O. K.; Hong, B. J.; Sarjeant, A. A.; Nguyen, S. T.; Hupp, J. T. Light-Harvesting Metal−Organic Frameworks (Mofs): Efficient Strut-to-Strut Energy Transfer in Bodipy and Porphyrin-Based Mofs. J. Am. Chem. Soc. 2011, 133, 15858−15861.
(24) Goswami, S.; Ma, L.; Martinson, A. B. F.; Wasielewski, M. R.; Farha, O. K.; Hupp, J. T. Toward Metal−Organic Framework-Based Solar Cells: Enhancing Directional Exciton Transport by Collapsing Three-Dimensional Film Structures. ACS Appl. Mater. Interfaces 2016, 8, 30863−30870.
(25) Kreno, L. E.; Leong, K.; Farha, O. K.; Allendorf, M.; Van Duyne, R. P.; Hupp, J. T. Metal−Organic Framework Materials as Chemical Sensors. Chem. Rev. 2012, 112, 1105−1125.
(26) Bai, Y.; Dou, Y.; Xie, L.-H.; Rutledge, W.; Li, J.-R.; Zhou, H.-C. Zr-Based Metal-Organic Frameworks: Design, Synthesis, Structure, and Applications. Chem. Soc. Rev. 2016, 45, 2327−2367.
(27) Howarth, A. J.; Buru, C. T.; Liu, Y.; Ploskonka, A. M.; Hartlieb, K. J.; McEntee, M.; Mahle, J. J.; Buchanan, J. H.; Durke, E. M.; Al-Juaid, S. S.; Stoddart, J. F.; Decoste, J. B.; Hupp, J. T.; Farha, O. K. Postsynthetic Incorporation of a Singlet Oxygen Photosensitizer in a Metal-Organic Framework for Fast and Selective Oxidative Detox-ification of Sulfur Mustard. Chem. - Eur. J. 2017, 23, 214−218.
(28) Zhang, W.-Q.; Li, Q.-Y.; Zhang, Q.; Lu, Y.; Lu, H.; Wang, W.; Zhao, X.; Wang, X.-J. Robust Metal−Organic Framework Containing Benzoselenadiazole for Highly Efficient Aerobic Cross-Dehydrogen-ative Coupling Reactions under Visible Light. Inorg. Chem. 2016, 55, 1005−1007.
(29) Li, R.; Wang, Z. J.; Wang, L.; Ma, B. C.; Ghasimi, S.; Lu, H.; Landfester, K.; Zhang, K. A. I. Photocatalytic Selective Bromination of Electron-Rich Aromatic Compounds Using Microporous Organic Polymers with Visible Light. ACS Catal. 2016, 6, 1113−1121.
(30) Gibson, G. L.; McCormick, T. M.; Seferos, D. S. Atomistic Band Gap Engineering in Donor−Acceptor Polymers. J. Am. Chem. Soc. 2012, 134, 539−547.
(31) Acharya, R.; Cekli, S.; Zeman, C. J.; Altamimi, R. M.; Schanze, K. S. Effect of Selenium Substitution on Intersystem Crossing in Π-Conjugated Donor−Acceptor−Donor Chromophores: The Lumo Matters the Most. J. Phys. Chem. Lett. 2016, 7, 693−697.
(32) Dolgopolova, E. A.; Williams, D. E.; Greytak, A. B.; Rice, A. M.; Smith, M. D.; Krause, J. A.; Shustova, N. B. A Bio-Inspired Approach for Chromophore Communication: Ligand-to-Ligand and Host-to-Guest Energy Transfer in Hybrid Crystalline Scaffolds. Angew. Chem., Int. Ed. 2015, 54, 13639−13643.
(33) Deria, P.; Yu, J.; Balaraman, R. P.; Mashni, J.; White, S. N. Topology-Dependent Emissive Properties of Zirconium-Based Por-phyrin Mofs. Chem. Commun. 2016, 52, 13031−13034.